PCCP

Accepted Manuscript

This is an *Accepted Manuscript*, which has been through the Royal Society of Chemistry peer review process and has been accepted for publication.

Accepted Manuscripts are published online shortly after acceptance, before technical editing, formatting and proof reading. Using this free service, authors can make their results available to the community, in citable form, before we publish the edited article. We will replace this *Accepted Manuscript* with the edited and formatted *Advance Article* as soon as it is available.

You can find more information about *Accepted Manuscripts* in the Information for Authors.

Please note that technical editing may introduce minor changes to the text and/or graphics, which may alter content. The journal's standard Terms & Conditions and the Ethical guidelines still apply. In no event shall the Royal Society of Chemistry be held responsible for any errors or omissions in this *Accepted Manuscript* or any consequences arising from the use of any information it contains.

ROYAL SOCIETY OF CHEMISTRY

www.rsc.org/pccp

Physical Chemistry Chemical Physics
CREATED USING THE RSC ARTICLE TEMPLATE (VER. 3.0) - SEE WWW.RSC.ORG/ELECTRONICFILES FOR DETAILS
ARTICLE TYPE www.rsc.org/xxxxxx | XXXXXXXX

Dynamic and Static Behavior of Hydrogen Bonds of the X–H---π Type (X = F, Cl, Br, I, RO and RR'N; R, R' = H or Me) in Benzene π-System, Elucidated by QTAIM Dual Functional Analysis

Yuji Sugibayashi,[a] Satoko Hayashi[a] and Waro Nakanishi*,[a]

Received (in XXX, XXX) 1st May 2015, Accepted XXX YYY 2015
First published on the web 1st May 2015
DOI: 10.1039/b000000x

Dynamic and static behavior of the X–H-∗-π interactions in X–H-∗-π(C_6H_6) (X = F, Cl, Br, I, HO, MeO, H_2N, MeHN and Me_2N) is elucidated by QTAIM-DFA (QTAIM dual functional analysis), which we proposed recently, as the first step to clarify various types of X–H-∗-π interactions. The asterisk ∗ emphasizes the existence of the bond critical point (BCP) on the interaction in question. Total electron energy densities ($H_b(\boldsymbol{r}_c)$) are plotted versus $H_b(\boldsymbol{r}_c) - V_b(\boldsymbol{r}_c)/2$ [= $(\hbar^2/8m)\nabla^2\rho_b(\boldsymbol{r}_c)$] at BCPs in QTAIM-DFA, where $V_b(\boldsymbol{r}_c)$ are potential energy densities at BCPs. In our treatment, data for the perturbed structures around the fully optimized ones are employed, in addition to those for the fully optimized structures. Data from the fully optimized structures are analyzed by the polar (R, θ) coordinate representation. Each plot for an interaction, containing data from the perturbed structures, shows a specific curve, which provides important information. The plot is expressed by (θ_p, κ_p): θ_p corresponds to the tangent line of the plot and κ_p is the curvature. θ and θ_p are measured from the y-axis and y-direction, respectively. While (R, θ) correspond to the static nature, (θ_p, κ_p) represent the dynamic nature of interactions. The nature of the X–H-∗-π(C_6H_6) interactions is well specified by (R, θ) and (θ_p, κ_p). All interactions, examined in this work, are classified by the pure closed shell interactions and predicted to have the van der Waals nature.

Introduction

Hydrogen atom (H) forms two center–two electron bonds of the σ-type (σ(2c–2e)) with other atoms (X), where one electron in σ(2c–2e) is supplied from the atomic 1s orbital of H and another one from the valence orbital of X. The H atom in H–X will be positively charged as in $H^{\delta+}$–$X^{\delta-}$, if the electronegativity of X (χ_X) is larger than that of H (χ_H) ($\chi_X > \chi_H$). Atoms of group 15, 16 and 17 elements, containing lone pair electrons (Z: or n(Z)), tend to interact with the polarized bonds at the positively charged $H^{\delta+}$ side of $H^{\delta+}$–$X^{\delta-}$, resulting in the formation of Z:---H–X. Such interactions are known as hydrogen bonds (HBs)[1–6] of the shared proton interaction type.[6,7] Conventional HBs of this type are formed with atoms of main group elements, X and Z,[6] which are usually not so strong in the neutral form (≤ 40 kJ mol^{-1}),[1,8] although they are usually stronger than the van der Waals (vdW) interactions. Attractive electrostatic interactions and the dispersion force mainly contribute to form vdW adducts. Contributions from the CT (charge transfer) interaction of the n(Z)→σ*($H^{\delta+}$–$X^{\delta-}$) type become more important as the strength of HBs increases, in addition to the vdW interactions.

HBs with the unsymmetric σ(3c–4e) character of the n(Z)---σ*($H^{\delta+}$–$X^{\delta-}$) type[7,9] will control the orientations of the HB adducts. Therefore, HBs play a very important role in all fields of chemical and biological sciences and they are fundamentally important by their ability of the molecular association due to the stabilization of the system in energy.[1–16] HBs also control various chemical processes depending on the strength. It must be a typical example that the duplex DNA structure once opens and then closes in active proliferation at around room temperature.[17] HBs will also play an important role in the very specific conformation of hormones, containing those in dimers, which controls the characteristic biological properties.[18] It must be inevitable to clarify the nature of HBs, for the better understanding the chemistry controlled by the interactions. We reported the behavior in conventional HBs of the shared proton interaction type by applying the quantum theory of atoms-in-molecules dual functional analysis (QTAIM-DFA), which we proposed recently.[19–21]

We also paid much attention to HBs of the X–H---π type, where π-electrons are supplied from acetylene,[22] ethylene,[23]

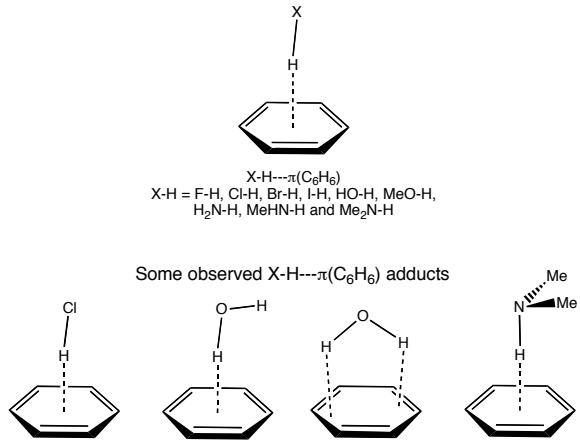

Scheme 1 Some X–H---π interactions in benzene π-system.

benzene[23] and related species.[25–27] Some structures of such adducts have been reported; the hydrogen chloride and hydrogen fluoride adducts of benzene and the derivatives by the microwave technics[28] and the interactions in benzene adduct with water by jet cooled microwave spectra[29] or Raman multivariate curve resolution (Raman-MCR),[30] and ammonia by microwave spectra[31] or infrared spectroscopy.[32–34] The Cl–H---π(C_6H_6) adduct has the C_1 symmetry close to C_s, where Cl–H is located near the D_{6h} axis of the original benzene.[28] Two types of H_2O adducts with benzene were reported, which would have the symmetries close to C_s and C_{2v}.[29] Scheme 1 illustrates the X–H---π interactions in X–H---π(C_6H_6) (X = F, Cl, Br, I, HO, MeO, H_2N, MeHN and Me_2N), to be elucidated in this work, together with some observed structures for the adducts.

QTAIM approach, introduced by Bader,[35,36] enables us to analyze the nature of chemical bonds and interactions.[35–39] Lots of QTAIM investigations have been reported so far,[35–58] however, those from a viewpoint of experimental chemists seem not so many. We proposed QTAIM-DFA, recently,[19–21] for experimental chemists, who are not so familiar with QTAIM, to analyze their own results, concerning chemical bonds and interactions, by their own image. QTAIM-DFA will provide an excellent possibility to evaluate, understand and classify weak to strong interactions in a unified form.[59]

Investigations on the X–H---π(C_6H_6) interactions have been growing successively.[22–34,60–71] However, it must be of very importance to clarify the causality between the basic properties of the interactions and the phenomena controlled by them, with physical necessity. We consider QTAIM-DFA to be well-suited to clarify the dynamic and static nature of the X–H---π(C_6H_6) interactions, in addition to the recent investigations on the behavior for conventional HBs of the shared proton interaction type.[8] Here, we present the results of theoretical elucidation of the X–H---π(C_6H_6) interactions with QTAIM-DFA, as the first step to clarify the behavior of various types of the X–H---π interactions.

QTAIM-DFA is surveyed next, together with the basic concept of the QTAIM approach.

QTAIM-DFA (QTAIM Dual Functional Analysis)

The bond critical point (BCP; $\boldsymbol{r}_c$, *[72]) is an important concept in QTAIM. BCP of $(\omega, \sigma) = (3, -1)$[35] is a point along the bond path (BP) at the interatomic surface, where charge density $\rho(\boldsymbol{r})$ reaches a minimum. A chemical bond or an interaction between A and B is denoted by A–B, which corresponds to BP between A and B in QTAIM. A-*-B emphasizes the existence of BCP in A–B.[35,72]

The sign of $\nabla^2\rho_b(\boldsymbol{r}_c)$ indicates that $\rho_b(\boldsymbol{r}_c)$ is depleted or concentrated with respect to its surrounding, since $\nabla^2\rho_b(\boldsymbol{r}_c)$ is the second derivative of $\rho(\boldsymbol{r})$ at BCP. $\rho_b(\boldsymbol{r}_c)$ is locally depleted relative to the average distribution around $\boldsymbol{r}_c$ if $\nabla^2\rho_b(\boldsymbol{r}_c) > 0$, but it is concentrated when $\nabla^2\rho_b(\boldsymbol{r}_c) < 0$. Total electron energy densities at BCPs ($H_b(\boldsymbol{r}_c)$) must be a more appropriate measure for weak interactions on the energy basis.[19–21,35,36,73] $H_b(\boldsymbol{r}_c)$ are the sum of kinetic energy densities ($G_b(\boldsymbol{r}_c)$) and potential energy densities ($V_b(\boldsymbol{r}_c)$) at BCPs, as shown in eqn (1). Electrons at BCPs are stabilized when $H_b(\boldsymbol{r}_c) < 0$, therefore, interactions exhibit the covalent nature in this region, whereas they exhibit no covalency if $H_b(\boldsymbol{r}_c) > 0$, due to the destabilization of electrons at BCPs under the conditions.[35] Eqn (2) represents the relation between $\nabla^2\rho_b(\boldsymbol{r}_c)$ and $H_b(\boldsymbol{r}_c)$, together with $G_b(\boldsymbol{r}_c)$ and $V_b(\boldsymbol{r}_c)$, which is closely related to the Virial theorem.

$$H_b(\boldsymbol{r}_c) = G_b(\boldsymbol{r}_c) + V_b(\boldsymbol{r}_c) \quad (1)$$

$$(\hbar^2/8m)\nabla^2\rho_b(\boldsymbol{r}_c) = H_b(\boldsymbol{r}_c) - V_b(\boldsymbol{r}_c)/2 = G_b(\boldsymbol{r}_c) + V_b(\boldsymbol{r}_c)/2 \quad (2)$$

Interactions are classified by the signs of $\nabla^2\rho_b(\boldsymbol{r}_c)$ and $H_b(\boldsymbol{r}_c)$. Interactions in the region of $\nabla^2\rho_b(\boldsymbol{r}_c) < 0$ are called shared-shell (SS) interactions and they are closed-shell (CS) interactions for $\nabla^2\rho_b(\boldsymbol{r}_c) > 0$. $H_b(\boldsymbol{r}_c)$ must be negative when $\nabla^2\rho_b(\boldsymbol{r}_c) < 0$, since $H_b(\boldsymbol{r}_c)$ are larger than $(\hbar^2/8m)\nabla^2\rho_b(\boldsymbol{r}_c)$ by $V_b(\boldsymbol{r}_c)/2$, where $V_b(\boldsymbol{r}_c) < 0$ at all BCPs (eqn (2)). Consequently, $\nabla^2\rho_b(\boldsymbol{r}_c) < 0$ and $H_b(\boldsymbol{r}_c) < 0$ are for the SS interactions. The CS interactions are especially called *pure* CS interactions for $H_b(\boldsymbol{r}_c) > 0$ and $\nabla^2\rho_b(\boldsymbol{r}_c) > 0$, since electrons at BCPs are depleted and destabilized under the conditions.[35a] Electrons in the intermediate region between SS and *pure* CS, which belong to CS, are locally depleted but stabilized at BCPs, since $\nabla^2\rho_b(\boldsymbol{r}_c) > 0$ but $H_b(\boldsymbol{r}_c) < 0$.[35a] We call the interactions in this region *regular* CS,[19–21] when it is necessary to distinguish from *pure* CS. The role of $\nabla^2\rho_b(\boldsymbol{r}_c)$ in the classification of interactions can be replaced by $H_b(\boldsymbol{r}_c) - V_b(\boldsymbol{r}_c)/2$, since $(\hbar^2/8m)\nabla^2\rho_b(\boldsymbol{r}_c) = H_b(\boldsymbol{r}_c) - V_b(\boldsymbol{r}_c)/2$ (eqn (2)).

We proposed QTAIM-DFA by plotting $H_b(\boldsymbol{r}_c)$ versus $H_b(\boldsymbol{r}_c) - V_b(\boldsymbol{r}_c)/2$ [$= (\hbar^2/8m)\nabla^2\rho_b(\boldsymbol{r}_c)$], after proposal of the plot of $H_b(\boldsymbol{r}_c)$ versus $\nabla^2\rho_b(\boldsymbol{r}_c)$.[19–21] Both axes in the plot of the former are given in energy unit, therefore, distances on the (x, y) (= $(H_b(\boldsymbol{r}_c) - V_b(\boldsymbol{r}_c)/2, H_b(\boldsymbol{r}_c))$ plane can be expressed in the energy unit. QTAIM-DFA incorporates the classification of interactions by the signs of $\nabla^2\rho_b(\boldsymbol{r}_c)$ and $H_b(\boldsymbol{r}_c)$ (*cf*: eqn (2)). Scheme 2 summarizes the proposal. Interactions of *pure* CS appear in the first quadrant, those of *regular* CS in the forth quadrant and data of SS drop in the third quadrant. No interactions appear in the second one.

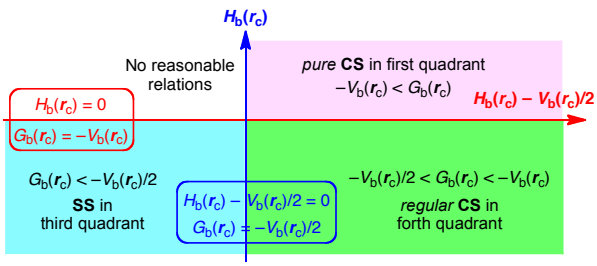

Scheme 2 QTAIM-DFA: Plot of $H_b(\boldsymbol{r}_c)$ versus $H_b(\boldsymbol{r}_c) - V_b(\boldsymbol{r}_c)/2$ for weak to strong interactions.

In our treatment, data for perturbed structures around fully-optimized structures are employed for the plots, in addition to the fully-optimized ones (see Fig. 1).[19–21,73] The method to generate the perturbed structures will be explained later. The plots of $H_b(\boldsymbol{r}_c)$ versus $H_b(\boldsymbol{r}_c) - V_b(\boldsymbol{r}_c)/2$ are analyzed employing the polar coordinate (R, θ) representation with the (θ_p, κ_p) parameters.[19a,20,21] Fig. 1 explains the treatment. R in (R, θ) is defined by eqn (3) and given in the energy unit. R corresponds

to the energy for an interaction at BCP. The plots show a spiral stream, as a whole.[19a,20,21] θ is defined by eqn (4) and measured from the y-axis, which controls the spiral stream of the plot and classifies the interactions. Each plot for an interaction gives a specific curve with the data from the perturbed structures and the fully-optimized one, which provides important information for the interaction. The curve is expressed by θ_p and κ_p. θ_p is defined by eqn (5) and measured from the y-direction, which corresponds to the tangent line of the plot. θ_p specifies the character of the interaction. κ_p is the curvature (eqn (6)).[19a]

We proposed the concept of "the dynamic nature of interactions" originated from the data containing the perturbed structures.[19a,20,21,73] While (R, θ) for the fully optimized structures correspond to the static nature, (θ_p, κ_p) exhibit the dynamic nature of interactions.[74] While $\rho(\boldsymbol{r})$, $\nabla^2\rho(\boldsymbol{r})$, $H(\boldsymbol{r}) - V(\boldsymbol{r})/2$, $H(\boldsymbol{r})$, $V(\boldsymbol{r})$ and $G(\boldsymbol{r})$ are called QTAIM functions, (R, θ) and (θ_p, κ_p) are QTAIM-DFA parameters, here. $k_b(\boldsymbol{r}_c)$, defined by eqn (7), is also an important QTAIM function. However, it will be treated as if it was a parameter, if suitable.

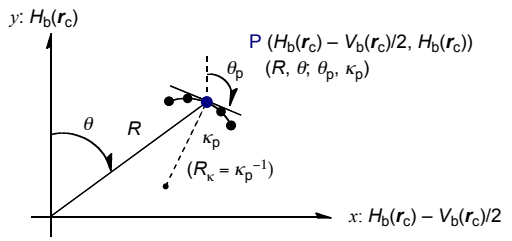

Fig. 1 Application of QTAIM-DFA. Polar (R, θ) coordinate representation with (θ_p, κ_p) for the plot of $H_b(\boldsymbol{r}_c)$ versus $H_b(\boldsymbol{r}_c) - V_b(\boldsymbol{r}_c)/2$.

$$R = (x^2 + y^2)^{1/2} \quad (3)$$
$$\theta = 90^\circ - \tan^{-1}(y/x) \quad (4)$$
$$\theta_p = 90^\circ - \tan^{-1}(dy/dx) \quad (5)$$
$$\kappa_p = |d^2y/dx^2| / [1 + (dy/dx)^2]^{3/2} \quad (6)$$
$$k_b(\boldsymbol{r}_c) = V_b(\boldsymbol{r}_c)/G_b(\boldsymbol{r}_c) \quad (7)$$
where $(x, y) = (H_b(\boldsymbol{r}_c) - V_b(\boldsymbol{r}_c)/2, H_b(\boldsymbol{r}_c))$

Application of QTAIM-DFA to Typical Interactions: Criteria to Classify and Characterize Interactions

OTAIM-DFA is applied to typical interactions; vdW, HBs, molecular complexes formed through CT (CT-MC), trihalide ions (X_3^-), trigonal bipyramidal adducts formed through CT (CT-TBP), weak covalent bonds (Cov-w) and strong covalent bonds (Cov-s). Rough criteria are obtained, after analysis of the plots, according to eqns (3)–(6).[19a,20,21] Scheme 3 shows

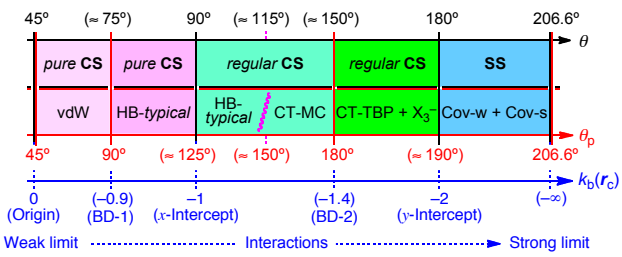

Scheme 3 Rough criteria to classify and characterize interactions by θ and θ_p. Values for $k_b(\boldsymbol{r}_c)$ are also given.

the rough criteria for the typical interactions.

Methodological Details in Calculations

Structures were optimized employing the Gaussian 09 program.[75] Various types of basis set systems (BSSs: BSS-A, BSS-B, BSS-C, BSS-D, BSS-E and BSS-F) were examined for the evaluations. Table 1 summarizes the BSSs. The basis set for I of the 6-311G* type[76] was obtained from EMSL Basis Set Exchange Library.[77,78] Higher basis set for I of the (7433211/743111/7411/2 + 1s1p1d1f) type was from Sapporo Basis Set Factory.[79] The diffusion functions of the *sp* parts for I in (7433211/743111/7411/2 + 1s1p1d1f)[80] were diverted as those of the *sp* type for the 6-311G* basis set of I, since the diffusion functions were not found for 6-311G* of I. The Møller-Plesset second order energy correlation (MP2) level was applied to all calculations.[81] Optimized structures were confirmed by the frequency analysis.

QTAIM functions were calculated using the Gaussian 09 program packages[75] with the same method of the optimizations and the data were analyzed with the AIM2000 program.[82] Normal coordinates of internal vibrations (NIV), obtained by the frequency analysis, were employed to generate the perturbed structures.[21,73] We call this method to generate the perturbed structures NIV. The method is explained in eqn (8). A k-th perturbed structure in question ($\mathbf{S}_{kw}$) is generated by the addition of the normal coordinates of the k-th internal vibration ($\mathbf{N}_k$) to the standard orientation of a fully-optimized structure ($\mathbf{S}_o$) in the matrix representation.[21] The coefficient f_{kw} in eqn (8) controls the difference in the structures between $\mathbf{S}_{kw}$ and $\mathbf{S}_o$: f_{kw} is determined to satisfy eqn (9) for the interaction distance in question (r) in a perturbed structure, where r_o is the distance in the fully-optimized structure, with a_o of Bohr radius (0.52918 Å).[83] $\mathbf{N}_k$ of five digits are used to predict $\mathbf{S}_{kw}$, although only two digits are usually printed out.[84] Perturbed structures generated with NIV correspond to those with r in question being elongated or shortened by $0.05a_o$ or $0.1a_o$, relative to r_o, (eqn (9)). NIV may also correspond to the photographic survey of the structures over the instantaneous ones of the selected motion in the zero-point internal vibrations by amplifying them to the extent where r in question satisfies eqn (9). The selected motion must be most effectively located on the interaction in question among the zero-point internal vibrations.

$$\mathbf{S}_{kw} = \mathbf{S}_o + f_{kw} \bullet \mathbf{N}_k \quad (8)$$
$$r = r_o + wa_o \quad (9)$$
(w = (0), ±0.05 and ±0.1; a_o = 0.52918 Å)
$$y = a_o + a_1x + a_2x^2 + a_3x^3 \quad (10)$$
(R_c^2: square of correlation coefficient)

In the QTAIM-DFA treatment, $H_b(r_c)$ are plotted versus $H_b(r_c) - V_b(r_c)/2$ for data of five points, where w = 0, ±0.05 and ±0.1 in eqn (9). Each plot is analyzed using a regression curve assuming the cubic function as shown in eqn (10), where $(x, y) = (H_b(r_c) - V_b(r_c)/2, H_b(r_c))$ ($R_c^2 > 0.99999$ in usual).[8,19–21,73]

The nature of the X–H-∗-π(C_6H_6) interactions will be discussed employing the criteria in Scheme 3, as a reference.

Table 1 Basis set systems employed for the calculations

BSS	C, H	F, Cl, Br	I
BSS-A	6-311G(d, p)	6-311G(d)	(5211111111/411111111/31111)[a]
BSS-B	6-311G(d, p)	6-311+G(d)	(5211111111/411111111/31111 + 1s1p)[b]
BSS-C	6-311G(d, p)	6-311G(3d)	(7433211/743111/7411/2 + 1s1p1d1f)[c]
BSS-D	6-311G(d, p)	6-311G(3df)	(7433211/743111/7411/2 + 1s1p1d1f)[c]
BSS-E	6-311G(d, p)	6-311+G(3df)	(7433211/743111/7411/2 + 1s1p1d1f)[c]
BSS-F	6-311++G(d, p)	6-311+G(3df)	(7433211/743111/7411/2 + 1s1p1d1f)[c]

[a] The basis set of the 6-311G* type for I was obtained from EMSL Basis Set Exchange Library.[77,78] [b] Diffusion functions of the 1s1p parts in (7433211/743111/7411/2 + 1s1p1d1f)[76] being employed as the diffusion functions of the 1s1p type for (5211111111/411111111/31111), which is called the 6-311G* basis set. [c] The higher basis set of the (7433211/743111/7411/2 + 1s1p1d1f) type for I was obtained from Sapporo Basis Set Factory.[79]

Table 2 Structural parameters for Cl–H---π(C_6H_6), evaluated with various basis set systems at the MP2 level[a]

BSS[b]	r(Cl, M[c])[d] (Å)	Δr(Cl, M[c])[e] (Å)	r(H, M[c]) (Å)	r(H, Cl) (Å)	∠MHCl[c] (°)
BSS-A	3.6285	-0.00_2	2.3705	1.2784	167.29
BSS-B	3.6053	-0.02_5	2.3320	1.2773	174.42
BSS-C	3.5659	-0.06_4	2.3292	1.2806	169.31
BSS-D	3.5516	-0.07_8	2.3178	1.2835	160.10
BSS-E	3.5470	-0.08_3	2.2778	1.2820	169.89
BSS-F	3.5740	-0.05_6	2.2924	1.2816	179.99

[a] The optimized structure was confirmed by all positive frequencies for each. [b] See Table 1 for BSSs. [c] A point M is placed at the center of C_6H_6 in Cl–H---π(C_6H_6). [d] The observed value for r(Cl, M) is 3.63 Å.[85] [e] Δr(Cl, M) = r_{calcd}(Cl, M) – r_{obsd}(Cl, M).

Results and Discussion

Optimization of Cl–H---π(C_6H_6) with Various BSSs

It must be important to employ such calculation method that reproduces well the observed structures for the better understanding the real picture of the interactions, since the picture drawn with QTAIM-DFA will change depending on the predicted distances. How do the calculation methods affect on the H---π distances in X–H---π(C_6H_6)? Optimizations were performed with BSS-X (X = A, B, C, D, E, and F) at the MP2 level, exemplified by Cl–H---π(C_6H_6) (see Table 1 for BSSs). The C_1 symmetry is confirmed for the optimized structures of Cl–H---π(C_6H_6) by the frequency analysis. The structural parameters are measured from a point M placed at the center of C_6H_6 in Cl–H---π(C_6H_6) (C_1). Table 2 collects those for Cl–H---π(C_6H_6) optimized with various BSSs.

The predicted r(Cl, M) distances become shorter in the order of BSS-A (3.629 Å) > BSS-B (3.605 Å) > BSS-F (3.574 Å) > BSS-C (3.566 Å) > BSS-D (3.552 Å) > BSS-E (3.547 Å) at the MP2 level. The r(Cl, M) values, determined by the microwave technics, is 3.63 Å.[85] The distances relative to the observed value, Δr(Cl, M) [= r_{calcd}(Cl, M) – r_{obsd}(Cl, M)], are also given in Table 2, which are -0.00_2, -0.02_5, -0.05_6, -0.06_4, -0.07_8 and -0.08_3 Å, respectively. The Δr(Cl, M) value seems more negative as the BSS level becomes higher, except for BSS-F. One may image that BSS-A is most suitable for the optimization of Cl–H---π(C_6H_6), relative to others, at first glance, together with BSS-B. However, the r(Cl, M) value of 3.574 Å predicted with BSS-F is the intermediate value between those predicted with BSS-C and BSS-B. Diffusion functions both on H and Cl would play an important role to reproduce the r(Cl, M) distances in the adduct.

The observed (assumed) r(H, Cl) value of 1.284 Å[85] is well reproduced by the predicted values of 1.277–1.284 Å. The ∠MHCl angles are predicted to be 160º–180º for Cl–H---π(C_6H_6), which are larger than the observed (estimated) value around 146º. The ∠MHCl angle must affect much on r(Cl, M) and r(H, M) in Cl–H---π(C_6H_6). The predicted r(H, M) values of 2.28–2.37 Å seem shorter than the observed value, which is expected to be around 2.50 Å, although it is obtained with some assumptions in the structural parameters.

The observed values would correspond to the averaged ones in the thermal processes, whereas the predicted values do to the minima on the energy surface at 0 K. The values change depending on the methods employed for the evaluation. Therefore, we must be careful when the predicted values are compared with the observed (estimated) ones. The observed value would change depending on the conditions of the measurement. The r(Cl, M) value in Cl–H---π(C_6H_6) could be shorter than that reported, since the temperature for the microwave measurements for Cl–H---π(C_6H_6) was around room temperature,[28] as usually. Namely, the r(Cl, M) and/or r(H, M) values determined under the experimental conditions could be longer than the intrinsic values.

Therefore, data evaluated with BSS-F are mainly employed for the discussion, together with others.[86] Data with BSS-A will cover the plausible range of the longer interaction distances, which could occur due to some unforeseen experimental conditions, such as strong solvent effect. On the other hand, those with BSS-D would supply the shorter distances, which may correspond to the strong limit of the X–H---π(C_6H_6) interaction under our calculation conditions.

Structural Optimizations of X–H---π(C_6H_6)

Structures of X–H---π(C_6H_6) (X = F, Cl, Br, I, HO, MeO, H_2N, MeHN and Me_2N) were optimized, employing BSS-A, BSS-B, BSS-D and/or BSS-F at the MP2 level. Optimized structures were confirmed by all positive frequencies through the frequency analysis. Scheme 4 summarizes the optimized

structures of X–H---π(C_6H_6). The structure will be called type I_{Bzn}, if only one X–H---π interaction is expected for each adduct, whereas the adduct will be type II_{Bzn}, if the structure is expected to contain two H---π interactions. The types of the structures will be employed to organize the optimized structures, therefore, they are independent from the molecular graphs constructed by BPs and BCPs. Type I_{Bzn} is sub-divided into type I_{Bzn}, type Ia_{Bzn} and type Iaa_{Bzn} for X in X–H of monovalent halogen, divalent oxygen and trivalent nitrogen atoms, respectively. While the type I_{Bzn}, type Ia_{Bzn} and type Iaa_{Bzn} structures will be denoted by X–H---π(C_6H_6), type II_{Bzn} will be OH_2---π(C_6H_6), where X–H = H–O–H.

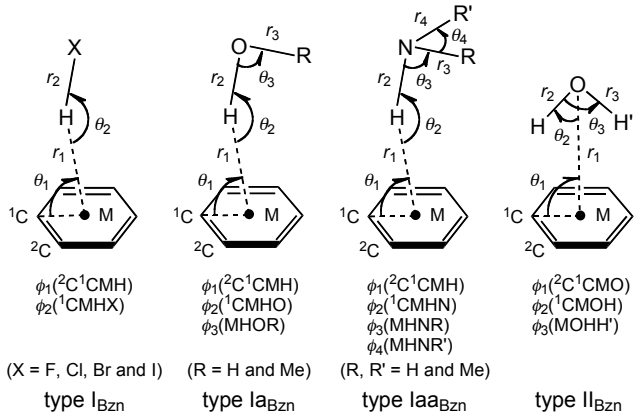

Scheme 4 Typical structures illustrated for X–H---π(C_6H_6).

Table 3 collects the structural parameters, r_1, r_2, r_3, r_4, θ_1, θ_2, θ_3, θ_4, ϕ_1, ϕ_2, ϕ_3 and/or ϕ_4 for X–H---π(C_6H_6), defined by Scheme 4, together with the symmetries and types. Optimized structures are not shown in a figure but some of them can be found in molecular graphs, since the molecular graphs are drawn on the optimized structures (see Fig. 3).

The optimized structures of X–H---π(C_6H_6) seem to change rather dramatically depending on the BSSs for X = F, Cl, Br and I, as shown in Table 3. The r_1 value for X–H---π(C_6H_6) predicted with BSS-D seems shortest, relative to those evaluated with other BSSs in Table 3, if the values of the same X (X = F, Cl, Br, and I) are compared. The results may show that r_1 is easily affected from the surrounding. The relative stability of the species should be strongly correlated to the r_1 values. On the other hand, the r_2 values seem very close with each other even if evaluated with various BSSs. The magnitudes of the differences are less than 0.01 Å, which shows that the X–H bonds would not be affected so easily in the formation of the adducts in benzene π-system.

The C_2 structure optimized for OH_2---π(C_6H_6) is predicted to have one imaginary (negative) frequency, in our calculation

Table 3 Structural parameters for X–H---C_6H_6, optimized with BSS-A, BSS-B, BSS-D and BSS-F at the MP2 level[a,b]

Species (Symmetry: type)	r_1 (Å)	r_2 (Å)	r_3 (Å)	r_4 (Å)	θ_1 (°)	θ_2 (°)	θ_3 (°)	ϕ_1 (°)	ϕ_2 (°)	ϕ_3 (°)	ΔE (kJ mol^{-1})
BSS-A											
F–H---π(C_6H_6) (C_s: type I_{Bzn})	2.2127	0.9170			78.8	155.3		-83.4	-149.3		-22.7
Cl–H---π(C_6H_6) (C_1: type I_{Bzn})	2.3705	1.2784			82.3	167.3		-88.3	-167.7		-18.2
Br–H---π(C_6H_6) (C_1: type I_{Bzn})	2.3466	1.4161			88.3	177.0		-90.0	-178.3		-18.7
I–H---π(C_6H_6) (C_s: type I_{Bzn})	2.3754	1.6085			87.4	173.2		-88.5	-150.0		-18.1
BSS-B											
F–H---π(C_6H_6) (C_s: type I_{Bzn})	2.3366	0.9219			76.1	165.5		-81.8	-149.0		-23.3
Cl–H---π(C_6H_6) (C_1: type I_{Bzn})	2.3320	1.2773			86.8	174.4		-89.4	-170.0		-20.7
Br–H---π(C_6H_6) (C_s: type I_{Bzn})	2.3323	1.4120			87.7	175.0		-88.7	-150.0		-20.6
I–H---π(C_6H_6) (C_1: type I_{Bzn})	2.3740	1.6086			86.0	170.7		-89.8	-177.3		-19.2
HO–H---π(C_6H_6) (C_s: type Ia_{Bzn})	2.4124	0.9619	0.9594		80.8	163.0	102.8	-84.7	-149.6	0.0	-17.8
OH_2---π(C_6H_6) (C_2: type II_{Bzn})[c]	3.2961	0.9610	0.9610		90.0	50.8	101.5	90.0	-30.0	0.0	-16.8
MeO–H---π(C_6H_6) (C_1: type Ia_{Bzn})	2.3150	0.9612	1.4178		82.7	166.8	106.9	85.8	149.7	0.0	-23.1
H_2N–H---π(C_6H_6) (C_s: type Iaa_{Bzn})[d]	2.4703	1.0143	1.0138	1.0138	83.6	176.1	107.1	-90.0	180.0	-57.2	-13.6
MeHN–H---π(C_6H_6) (C_1: type Iaa_{Bzn})[e]	2.3982	1.0142	1.4636	1.0144	84.5	162.0	109.8	87.1	117.4	-11.4	-18.9
Me_2N–H---π(C_6H_6) (C_1: type Iaa_{Bzn})[f]	2.3174	1.0140	1.4559	1.4559	85.2	158.3	108.9	87.2	149.9	-60.8	-25.5
BSS-D											
F–H---π(C_6H_6) (C_1: type I_{Bzn})	2.1638	0.9196			76.9	154.9		90.0	179.9		-25.1
Cl–H---π(C_6H_6) (C_1: type I_{Bzn})	2.3178	1.2835			80.0	160.1		-85.3	-154.6		-21.5
Br–H---π(C_6H_6) (C_1: type I_{Bzn})	2.3113	1.4201			83.0	165.4		-86.4	-152.4		-22.3
I–H---π(C_6H_6) (C_1: type I_{Bzn})	2.2871	1.6159			81.4	156.7		-89.8	-178.5		-27.9
BSS-F											
F–H---π(C_6H_6) (C_s: type I_{Bzn})	2.2902	0.9252			78.1	165.0		-83.0	-149.2		-24.0
Cl–H---π(C_6H_6) (C_s: type I_{Bzn})	2.2924	1.2816			90.0	180.0		-90.0	180.0		-24.0
Br–H---π(C_6H_6) (C_{6v}: type I_{Bzn})	2.3151	1.4193			90.0	180.0		-90.0	180.0		-23.8
I–H---π(C_6H_6) (C_s: type I_{Bzn})	2.2934	1.6153			84.8	166.8		-90.0	180.0		-27.3
HO–H---π(C_6H_6) (C_s: type Ia_{Bzn})	2.3824	0.9635	0.9607		81.7	166.5	104.2	-85.1	-149.6	0.0	-18.7
OH_2---π(C_6H_6) (C_2: type II_{Bzn})[c]	3.3195	0.9623	0.9623		90.0	51.5	103.0	90.0	-30.0	0.0	-17.2
MeO–H---π(C_6H_6) (C_s: type Ia_{Bzn})	2.2771	0.9628	1.4200		83.3	167.3	108.3	-86.1	-149.8	0.0	-24.6
H_2N–H---π(C_6H_6) (C_s: type Iaa_{Bzn})[g]	2.4375	1.0153	1.0145	1.0145	84.8	179.2	106.7	-90.0	180.0	-56.9	-14.9
MeHN–H---π(C_6H_6) (C_1: type Iaa_{Bzn})[h]	2.3624	1.0144	1.4614	1.0144	84.9	163.2	110.0	-87.6	169.7	-14.1	-20.8
Me_2N–H---π(C_6H_6) (C_1: type Iaa_{Bzn})[i]	2.2792	1.0139	1.4526	1.4526	85.2	159.5	109.0	87.3	150.1	-61.2	-27.6

[a] See Table 1 for BSSs. [b] $\Delta E = E$ (X–H-*-π(C_6H_6)) – (E (X–H) + E (C_6H_6)). [c] One imaginary frequency being predicted for the adduct. [d] (θ_4, ϕ_4) = (107.0°, 57.2°). [e] (θ_4, ϕ_4) = (110.0°, 107.7°). [f] (θ_4, ϕ_4) = (111.3°, 60.8°). [g] (θ_4, ϕ_4) = (106.6°, 56.9°). [h] (θ_4, ϕ_4) = (110.3°, 105.3°). [i] (θ_4, ϕ_4) = (111.8°, 61.2°).

system. It should be assigned to a transition state (TS). A C_1 structure very close to the C_2 structure was also optimized, if the optimization is started assuming the C_1 symmetry. One imaginary frequency was predicted again to the species. Very gradual energy surface around the motion would be responsible for the imaginary frequency under the calculation conditions. All positive frequencies could be predicted for OH_2---π(C_6H_6) (C_2: type II_{Bzn}), if the calculation system is suitably selected. Further investigations seem necessary, which will be discussed in the forthcoming paper.

How are the species stabilized? Table 3 also contains the stabilization energies ΔE in the formation of X–H---π(C_6H_6) [$\Delta E = E$ (X–H---π(C_6H_6)) – (E (X–H) + E (C_6H_6))), where the structures of the components, X–H and C_6H_6, are assumed to be the same as those in X–H---π(C_6H_6). The ΔE values evaluated with BSS-A, BSS-D and BSS-F at the MP2 level (abbreviated by ΔE_A, ΔE_D and ΔE_F, respectively) are plotted versus ΔE_B, separately by (X = F, Cl, Br and I) and (X = HO, MeO, H_2N, MeHN and Me_2N) to examine the trend in ΔE. Fig. 2 shows the results. The plots gave good correlations, which were given in the figure with the square of the correlation coefficient (R_c^2). Data for I–H---π(C_6H_6) in ΔE_D and ΔE_F deviated downward from the corresponding correlation lines. Higher basis set for I employed to evaluate ΔE_D and ΔE_F would be responsible for the deviations, relative to the case of ΔE_B. The data were omitted in the correlations. While ΔE_F for X–H---π(C_6H_6) (X = HO, MeO, H_2N, MeHN and Me_2N) correlated well with ΔE_B, ΔE_F for X–H---π(C_6H_6) (X = F, Cl and Br) were predicted to be very close values of about 24 kJ mol^{-1}. The ΔE values must be mainly controlled by the r_1 values, which would also be much affected from the surrounding in the formation of the adducts.

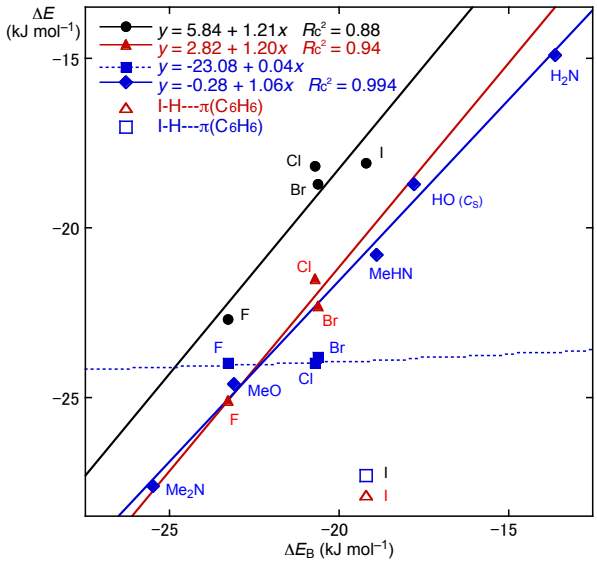

Fig. 2 Plots of ΔE_A (●), ΔE_D (▲/△) and ΔE_F (■/□) versus ΔE_B for X–H--π(C_6H_6) (X = F, Cl, Br and I) with ΔE_F (◆) versus ΔE_B for X = HO, MeO, H_2N, MeHN and Me_2N). Data for I–H---π(C_6H_6) deviated from the correlations in ΔE_D and ΔE_F, which are shown by △ and □, respectively.

Before application of QTAIM-DFA to X–H---π(C_6H_6), molecular graphs, counter maps, negative Laplacians and trajectory plots were examined, first.

Molecular Graphs, Counter Maps, Negative Laplacians and Trajectory Plots for X–H-∗-π(C_6H_6)

Fig. 3 illustrates the molecular graphs for X–H-∗-π(C_6H_6) (X = F, Br, I, HO, MeO, H_2N and Me_2N) evaluated with BSS-F, together with Br–H-∗-π(C_6H_6) and MeO–H-∗-π(C_6H_6) calculated with BSS-B, at the MP2 level. All BCPs expected are clearly detected, containing those for the X–H-∗-π(C_6H_6) interactions, together with ring critical points (RCPs) and cage critical points (CCPs). Each H of X–H in X–H-∗-π(C_6H_6) is connected to π(C_6H_6) by BP with BCP. Therefore, main interactions in X–H-∗-π(C_6H_6) should be of the H-∗-π type, although additional interactions between C in Me and π(C_6H_6) are detected in MeO–H-∗-π(C_6H_6) (C_1: type Ia_{Bzn}), if evaluated with BSS-B. The molecular graphs of X–H---π(C_6H_6) may change topologically depending on BSSs employed for the evaluations. The symmetry in the optimized structures must be an important factor for the change in molecular graphs of X–H---π(C_6H_6) (see, Figs. 3b and 3i for Br–H-∗-π(C_6H_6)).

Fig. 4 draws the counter maps of $\rho(\boldsymbol{r})$ drawn on the C_s plane or that close to the plane of the adducts, exemplified by X–H-∗-π(C_6H_6) (X = Br, I, HO, MeO, H_2N and Me_2N) and OH_2---π(C_6H_6) evaluated with BSS-F, together with MeO–H-∗-π(C_6H_6) calculated with BSS-B. BCPs are well located at the three-dimensional saddle points of $\rho(\boldsymbol{r})$. Figs. 5 and 6 show the negative Laplacians and trajectory plots, respectively, for the same adducts drawn in Fig. 4. It is well visualized how BCPs are classified through $\nabla^2\rho(\boldsymbol{r})$ (Fig. 5) and the space around the species is well divided into atoms in each adduct (Fig. 6).

QTAIM functions are calculated at BCPs of X–H-∗-π(C_6H_6) and QTAIM-DFA is applied to the interactions to clarify the behavior. The results are discussed next.

Survey of the X–H-∗-π(C_6H_6) Interactions.

Before discussion of the behavior of X–H-∗-π(C_6H_6), it is instructive to examine BPs for the interactions, since some BPs are apparently curved, as shown in Fig. 3. Therefore, the lengths of BPs (r_{BP}) will be substantially longer than the corresponding straight-line distances (R_{SL}). The r_{BP} values and the components (r_{BP1} and r_{BP2}: $r_{BP} = r_{BP1} + r_{BP2}$) in question are collected in Table S1 of the Supporting Information, together with the R_{SL} values, where r_{BP1} and r_{BP2} are those between H in XH and BCP in question and between the BCP and a point in C_6H_6 in question, respectively.

Fig. 7 shows the plot of r_{BP} *versus* R_{SL} for X–H-∗-π(C_6H_6), evaluated with BSS-F at the MP2 level. It is demonstrated that r_{BP} are very close to R_{SL} ($0.020 \le r_{BP} - R_{SL} \le 0.034$ Å), except for MeHN–H-∗-π(C_6H_6) (C_1: type Iaa_{Bzn}) and Me_2N–H-∗-π(C_6H_6) (C_1: type Iaa_{Bzn}) of which $r_{BP} - R_{SL}$ values amount to 0.56–0.58 Å. Consequently, the X–H-∗-π(C_6H_6) interactions can be described by the linear BPs, except for the two. In the case of MeHN–H-∗-π(C_6H_6) (C_1: type Iaa_{Bzn}) and Me_2N–H-∗-π(C_6H_6) (C_1: type Iaa_{Bzn}), the BPs are expected to connect H in MeRN–H (R = H and Me) and BCP of C=C in C_6H_6, from the geometric feature, at first glance. However, it is recognized that BPs connect H in MeRN–H (R = H and Me) and C in C_6H_6, after careful examination. The results must be

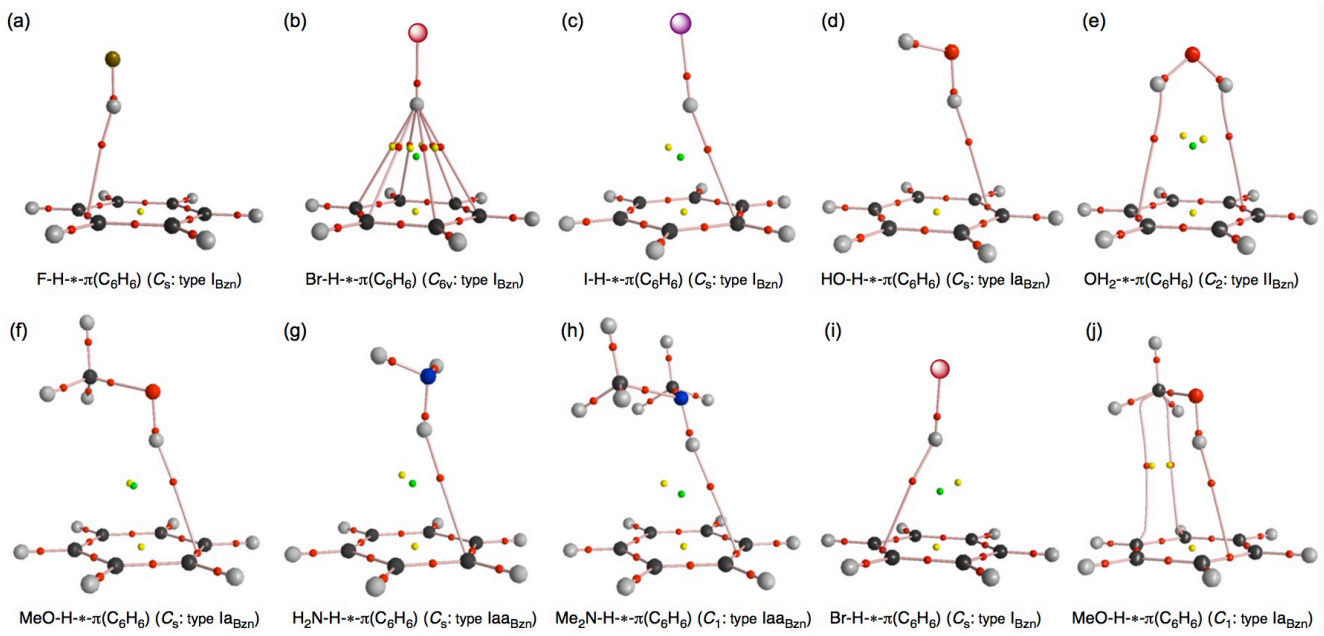

Fig. 3 Molecular graphs for F–H-∗-π(C_6H_6) (C_s: type I_{Bzn}) (a), Br–H-∗-π(C_6H_6) (C_{6v}: type I_{Bzn}) (b), I–H-∗-π(C_6H_6) (C_s: type I_{Bzn}) (c), HO–H-∗-π(C_6H_6) (C_s: type Ia_{Bzn}) (d), OH_2-∗-π(C_6H_6) (C_2: type II_{Bzn}) (e), MeO–H-∗-π(C_6H_6) (C_s: type I_{Bzn}) (f), H_2N–H-∗-π(C_6H_6) (C_s: type Iaa_{Bzn}) (g) and Me_2N–H-∗-π(C_6H_6) (C_1: type Iaa_{Bzn}) (h), evaluated with BSS-F, together with Br–H-∗-π(C_6H_6) (C_s: type I_{Bzn}) (i) and MeO–H-∗-π(C_6H_6) (C_1: type Ia_{Bzn}) (j) evaluated by BSS-B. BCPs are denoted by red dots (●), RCPs by yellow dots (●) and CCPs by green dots (●), together with BPs by pink line (-●-). Carbon atoms are in black (●) and hydrogen atoms in gray (●), with fluorine, bromine and iodine atoms in dark gold (●), brown (●) and purple (●), respectively.

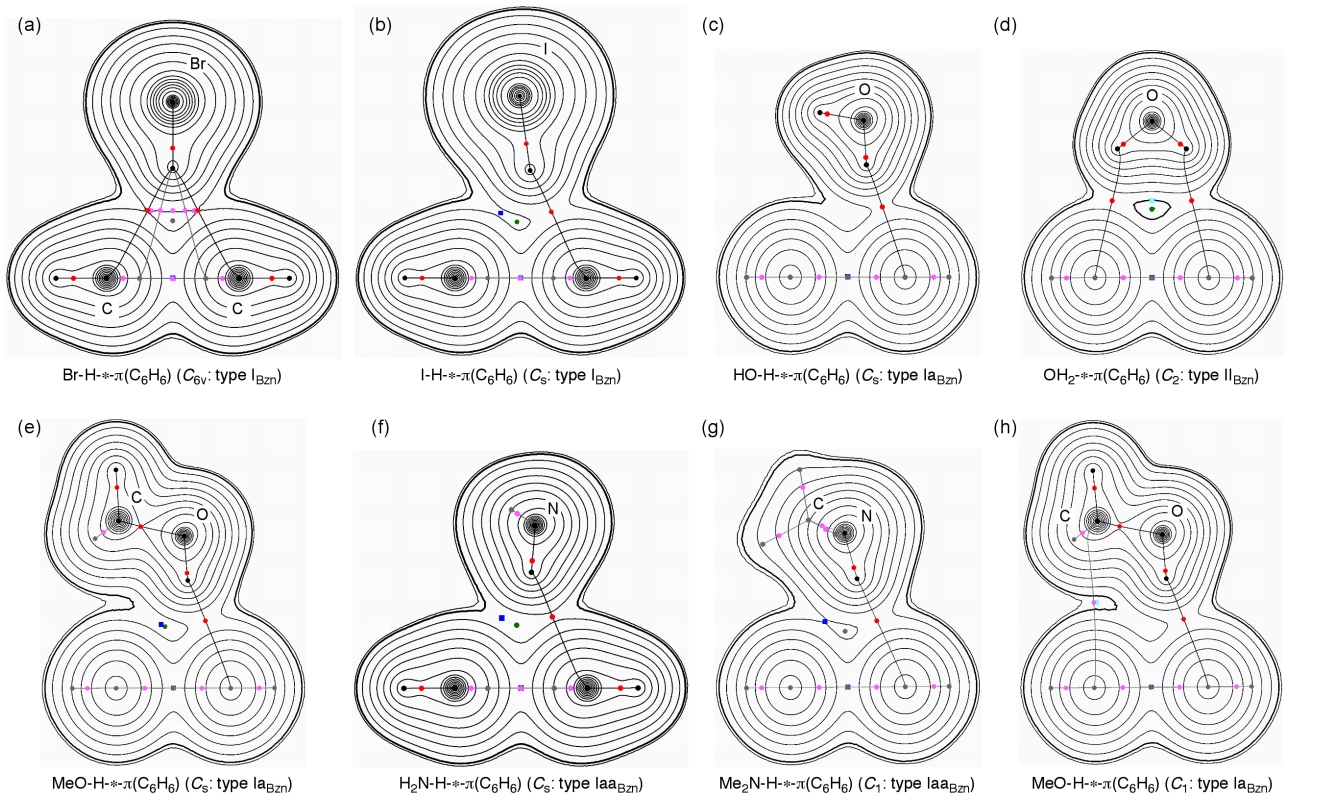

Fig. 4 Counter maps of $\rho_b(\boldsymbol{r}_c)$ for Br–H-∗-π(C_6H_6) (C_{6v}: type I_{Bzn}) (a), I–H-∗-π(C_6H_6) (C_s: type I_{Bzn}) (b), HO–H-∗-π(C_6H_6) (C_s: type Ia_{Bzn}) (c), OH_2-∗-π(C_6H_6) (C_2: type II_{Bzn}) (d), MeO–H-∗-π(C_6H_6) (C_s: type Ia_{Bzn}) (e), H_2N–H-∗-π(C_6H_6) (C_s: type Iaa_{Bzn}) (f) and Me_2N–H-∗-π(C_6H_6) (C_1: type Iaa_{Bzn}) (g) evaluated with BSS-F, together with MeO–H-∗-π(C_6H_6) (C_1: type Ia_{Bzn}) (h) calculated by BSS-B. BCPs on the plane are denoted by red dots (●), those outside of the plane in pink dots (●), RCPs by blue squares (■), CCPs by green dots (■) and BPs on the plane by black lines and those outside of the plane are by gray lines. Carbon atoms are in black (●) and hydrogen atoms are in gray (●), with other atoms in black (●).

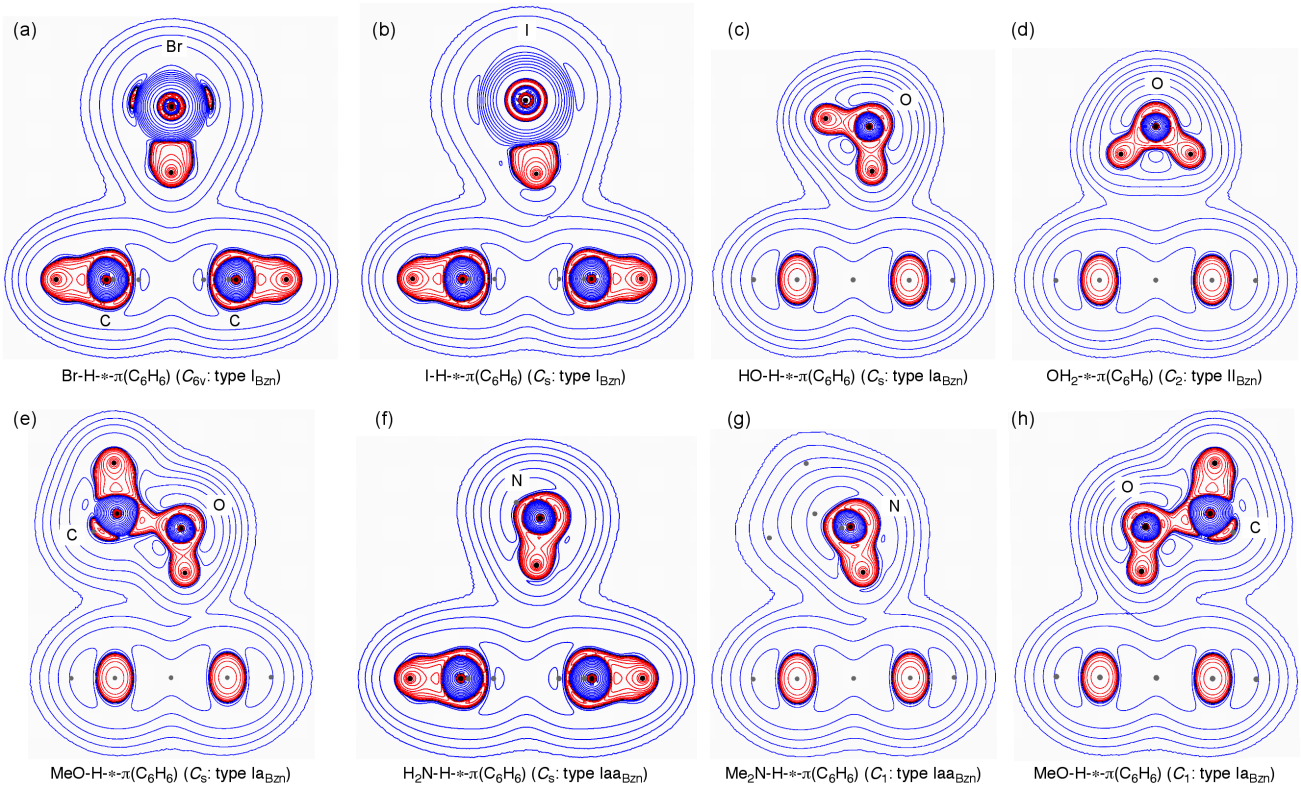

Fig. 5 Negative Laplacians for Br–H-∗-π(C_6H_6) (C_{6v}: type I_{Bzn}) (a), I–H-∗-π(C_6H_6) (C_s: type I_{Bzn}) (b), HO–H-∗-π(C_6H_6) (C_s: type Ia_{Bzn}) (c), OH_2-∗-π(C_6H_6) (C_2: type II_{Bzn}) (d), MeO–H-∗-π(C_6H_6) (C_s: type Ia_{Bzn}) (e), H_2N–H-∗-π(C_6H_6) (C_s: type Iaa_{Bzn}) (f) and Me_2N–H-∗-π(C_6H_6) (C_1: type Iaa_{Bzn}) (g), evaluated with BSS-F, together with MeO–H-∗-π(C_6H_6) (C_1: type Ia_{Bzn}) (h) by BSS-B. Blue and red lines correspond to positive and negative areas, respectively.

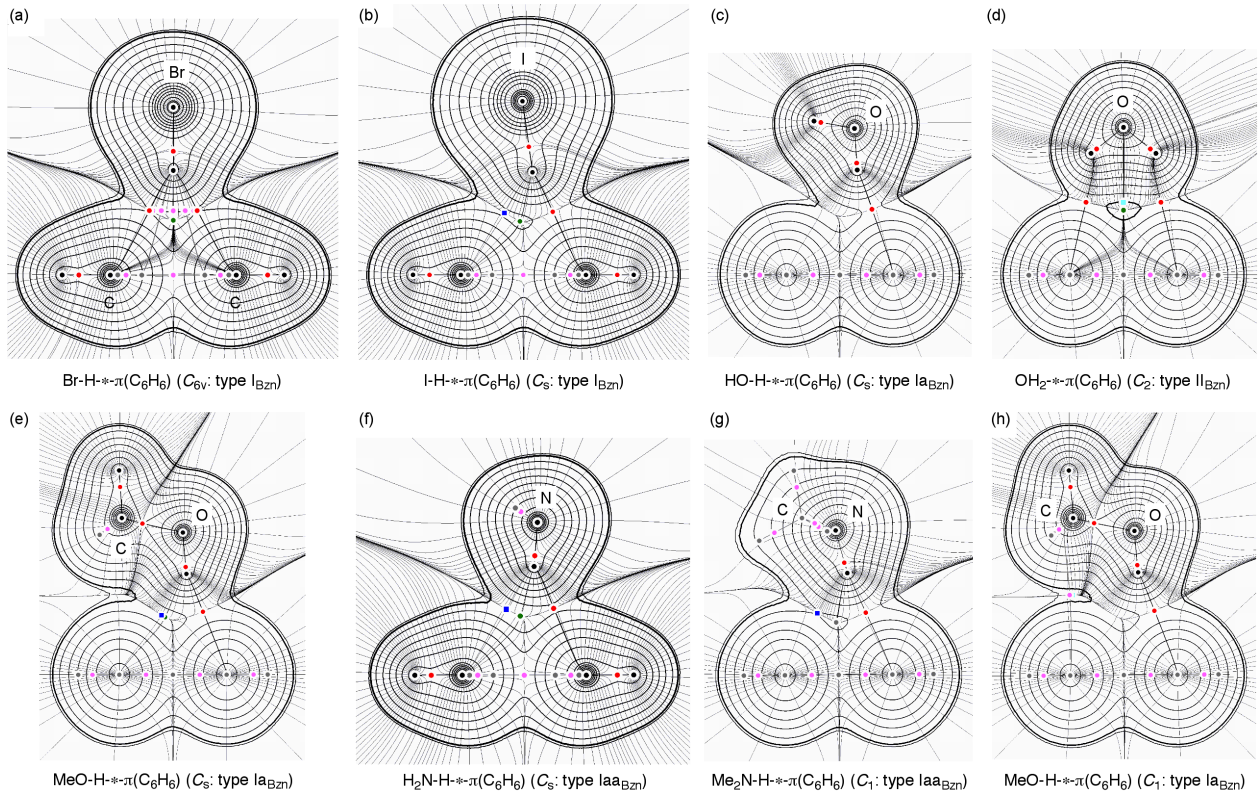

Fig. 6 Trajectory plots for Br–H-∗-π(C_6H_6) (C_{6v}: type I_{Bzn}) (a), I–H-∗-π(C_6H_6) (C_s: type I_{Bzn}) (b), HO–H-∗-π(C_6H_6) (C_s: type Ia_{Bzn}) (c), OH_2-∗-π(C_6H_6) (C_2: type II_{Bzn}) (d), MeO–H-∗-π(C_6H_6) (C_s: type Ia_{Bzn}) (e), H_2N–H-∗-π(C_6H_6) (C_s: type Iaa_{Bzn}) (f) and Me_2N–H-∗-π(C_6H_6) (C_1: type Iaa_{Bzn}) (g), evaluated with BSS-F, together with MeO–H-∗-π(C_6H_6) (C_1: type Ia_{Bzn}) (h) by BSS-B. Colors and marks are the same as those in Fig. 3.

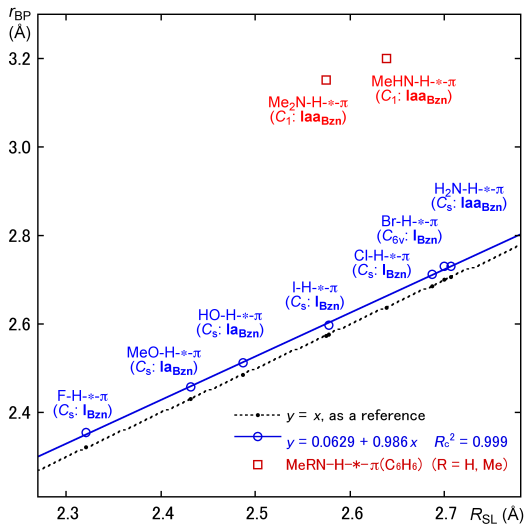

Fig. 7 Plot of r_{BP} versus R_{SL} evaluated with BSS-F at the MP2 level. Correlation for type I_{Bzn} with X = F, Cl, Br, I, HO, MeO and H_2N is given in the figure, together with R_c^2 (the square of the correlation coefficient).

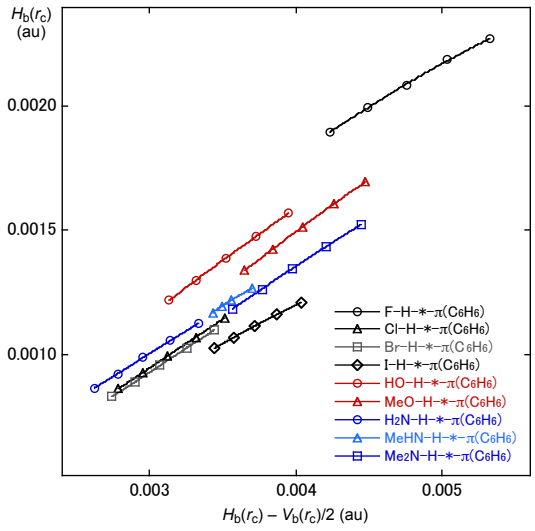

Fig. 8 Plots of $H_b(\boldsymbol{r}_c)$ versus $H_b(\boldsymbol{r}_c) - V_b(\boldsymbol{r}_c)/2$ for X–H-∗-π(C_6H_6), evaluated with BSS-F at the MP2 level. Colors and marks for the species are shown in the figure. Data with w = –0.1, –0.05, –0.025, (0) and 0.001 are employed for MeHN–H-∗-π(C_6H_6), in place of those with w = (0), ±0.05 and ±0.1, resulting in narrower intervals between the data points on the regression curves for the species, relative to others.

responsible for the larger differences between r_{BP} and R_{SL} for the species.

QTAIM-DFA is applied to X–H-∗-π(C_6H_6) (X–H = F, Cl, Br, I, HO, MeO, H_2N, MeHN and Me_2N). Fig. 8 shows the plots of $H_b(\boldsymbol{r}_c)$ versus $H_b(\boldsymbol{r}_c) - V_b(\boldsymbol{r}_c)/2$ for the X–H-∗-π(C_6H_6) interactions, evaluated with BSS-F. All data in Fig. 8 appear in the area of $H_b(\boldsymbol{r}_c) - V_b(\boldsymbol{r}_c)/2 > 0$ and $H_b(\boldsymbol{r}_c) > 0$, which belong to the *pure* CS region. Therefore, all H-∗-π interactions in X–H-∗-π(C_6H_6) should be classified by *pure* CS interactions.

The plots are analyzed according to eqns (3)–(6) by applying QTAIM-DFA. The results are discussed, next.

Application of QTAIM-DFA to X–H-∗-π(C_6H_6) Interactions

Table 4 collects the QTAIM-DFA parameters, evaluated with BSS-A, BSS-B, BSS-D and BSS-F at the MP2 level. The behavior of the X–H-∗-π(C_6H_6) interactions are classified and characterized based on the QTAIM-DFA parameters of θ and θ_p, respectively, employing the criteria in Scheme 3, as a reference. The criteria tell us that the interactions will be classified by the *pure* CS interactions if 45° < θ < 90° and characterized as the vdW interactions for 45° ≤ θ_p < 90°. The θ and θ_p values are less than 90° for all X–H-∗-π(C_6H_6), examined in this work, as shown in Table 4. Consequently, all X–H-∗-π(C_6H_6) interactions are classified as the *pure* CS interactions and they have the vdW-*type* character, where X = F, Cl, Br, I, HO, MeO, H_2N, MeHN and Me_2N.

How are the trends in the behavior of θ and θ_p in X–H-∗-π(C_6H_6)? To clarify the trends, θ and θ_p in X–H-∗-π(C_6H_6) and X–H-∗-n(OH_2) are plotted versus X (= F, Cl, Br and I) in Fig. 9, evaluated with BSS-F at the MP2 level. While θ in X–H-∗-π(C_6H_6) become larger in the order of X = F < Cl < Br < I, θ_p increase in the order of X = Cl ≤ Br (< F) < I. The behavior seems inverse in the trend of X–H-∗-OH_2, as a whole.[8,87]

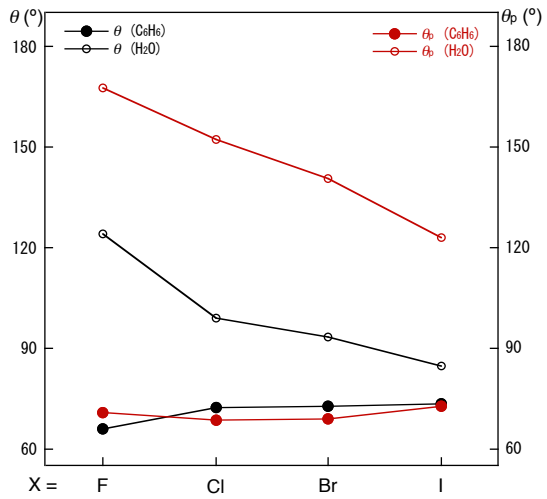

Fig. 9 Plots of θ versus X (= F, Cl, Br and I) for X–H-∗-π(C_6H_6) (●) and X–H-∗-n(OH_2) (○) and those of θ_p versus X for X–H-∗-π(C_6H_6) (●) and X–H-∗-n(OH_2) (○) evaluated with BSS-F at the MP2 level.

What factors control the trends? Acidity of H–X[88] and MO energies of σ*(X–H) would be the candidates for the factors. The acidity of H–X in the gas phase and ε(LUMO) of H–X[89] are given in eqns (11) and (12), respectively. The acidity becomes stronger in the order of X = F < Cl < Br < I, as expected (eqn (11)). The θ and θ_p values in X–H-∗-π(C_6H_6) increase almost proportionally as the acidity of H–X becomes stronger. However, those in X–H-∗-n(OH_2) change inversely proportional to the acidity of H–X, as visualized in Fig. 9. Instead, ε(LUMO) of H–X seems to explain the behavior of θ and θ_p in X–H-∗-n(OH_2), as a whole, although ε(LUMO) of H–Cl is predicted to be less than that of H–F.

Acidity (ΔH^o/kJ mol^{-1}):

HF (–1552) < HCl (–1396) < HBr (–1351) < HI (–1315) (11)

ε(LUMO) of H–X (eV):

HCl (1.12) < HF (1.17) ≤ HBr (1.18) < HI (1.25) (12)

Table 4 QTAIM functions and QTAIM-DFA parameters for X–H---π(C_6H_6), optimized with MP2/BSS-A, MP2/BSS-B, MP2/BSS-D and MP2/BSS-F at the MP2 level[a,b]

Species (Symmetry: type)	BCP at C_6H_6	$\rho_b(\boldsymbol{r}_c)$ (ea_o^{-3})	$c\nabla^2\rho_b(\boldsymbol{r}_c)^c$ (au)	$H_b(\boldsymbol{r}_c)$ (au)	$k_b(\boldsymbol{r}_c)^d$	R (au)	θ (°)	Freq (cm^{-1})	k_f (unit[e])	θ_p (º)	κ_p (au^{-1})
BSS-A											
F–H-∗-π(C_6H_6) (C_s: type I_{Bzn})	BCP	0.0121	0.0054	0.0024	-0.717	0.0059	66.2	112.7	0.053	72.3	136
Cl–H-∗-π(C_6H_6) (C_1: type I_{Bzn})	C	0.0091	0.0033	0.0010	-0.824	0.0035	73.3	76.4	0.030	67.1	20.5
Br–H-∗-π(C_6H_6) (C_1: type I_{Bzn})	C	0.0080	0.0030	0.0008	-0.843	0.0031	74.8	64.0	0.021	69.5	59.2
I–H-∗-π(C_6H_6) (C_s: type I_{Bzn})	BCP	0.0084	0.0030	0.0008	-0.852	0.0031	75.5	38.6	0.002	71.6	351
BSS-B											
F–H-∗-π(C_6H_6) (C_s: type I_{Bzn})	BCP	0.0113	0.0048	0.0021	-0.717	0.0052	66.2	110.1	0.057	70.7	109
Cl–H-∗-π(C_6H_6) (C_1: type I_{Bzn})	C	0.0083	0.0031	0.0009	-0.831	0.0032	73.9	81.2	0.032	67.3	30.2
Br–H-∗-π(C_6H_6) (C_s: type I_{Bzn})	BCP	0.0087	0.0031	0.0009	-0.834	0.0032	74.1	64.2	0.017	67.6	74.4
I–H-∗-π(C_6H_6) (C_1: type I_{Bzn})	C	0.0087	0.0031	0.0008	-0.856	0.0032	75.9	44.6	0.003	73.5	208
HO–H-∗-π(C_6H_6) (C_s: type Ia_{Bzn})	BCP	0.0085	0.0035	0.0013	-0.761	0.0037	68.9	101.8	0.027	64.2	35.9
MeO–H-∗-π(C_6H_6) (C_1: type Ia_{Bzn})	BCP	0.0093	0.0039	0.0015	-0.767	0.0042	69.3	84.5	0.012	64.7	74.3
H_2N–H-∗-π(C_6H_6) (C_s: type Iaa_{Bzn})	C	0.0072	0.0029	0.0009	-0.808	0.0030	72.2	96.5	0.027	68.2	3.4
MeHN–H-∗-π(C_6H_6) (C_1: type Iaa_{Bzn})	C	0.0081	0.0033	0.0011	-0.805	0.0035	71.9	109.0	0.009	71.2	224
Me_2N–H-∗-π(C_6H_6) (C_1: type Iaa_{Bzn})	C	0.0091	0.0037	0.0012	-0.804	0.0039	71.9	87.8	0.018	67.3	22.0
BSS-D											
F–H-∗-π(C_6H_6) (C_1: type I_{Bzn})	C	0.0133	0.0059	0.0023	-0.756	0.0063	68.6	124.9	0.066	83.2	204
Cl–H-∗-π(C_6H_6) (C_1: type I_{Bzn})	C	0.0110	0.0042	0.0015	-0.788	0.0044	70.7	81.6	0.030	69.2	92.5
Br–H-∗-π(C_6H_6) (C_1: type I_{Bzn})	C	0.0102	0.0039	0.0013	-0.801	0.0041	71.6	62.7	0.016	68.5	58.2
I–H-∗-π(C_6H_6) (C_1: type I_{Bzn})	C	0.0115	0.0042	0.0012	-0.824	0.0044	73.3	69.6	0.014	75.0	122
BSS-F											
F–H-∗-π(C_6H_6) (C_s: type I_{Bzn})	BCP	0.0110	0.0047	0.0021	-0.714	0.0051	66.0	105.9	0.054	70.7	109
Cl–H-∗-π(C_6H_6) (C_s: type I_{Bzn})	C	0.0077	0.0031	0.0010	-0.811	0.0033	72.3	88.7	0.052	68.5	2.2
Br–H-∗-π(C_6H_6) (C_{6v}: type I_{Bzn})	C	0.0078	0.0031	0.0010	-0.816	0.0032	72.7	69.3	0.031	68.8	1.7
I–H-∗-π(C_6H_6) (C_s: type I_{Bzn})	C	0.0101	0.0037	0.0011	-0.824	0.0039	73.3	63.8	0.010	72.5	83.0
HO–H-∗-π(C_6H_6) (C_s: type Ia_{Bzn})	BCP	0.0085	0.0035	0.0014	-0.754	0.0038	68.5	102.0	0.034	66.6	39.0
MeO–H-∗-π(C_6H_6) (C_s: type Ia_{Bzn})	BCP	0.0096	0.0040	0.0015	-0.769	0.0043	69.5	85.2	0.014	66.4	57.9
H_2N–H-∗-π(C_6H_6) (C_s: type Iaa_{Bzn})	C	0.0072	0.0030	0.0010	-0.800	0.0031	71.5	97.4	0.028	69.7	7.9
MeHN–H-∗-π(C_6H_6) (C_1: type Iaa_{Bzn})	C	0.0083	0.0034	0.0012	-0.795	0.0036	71.2	68.1	0.010	65.5	923
Me_2N–H-∗-π(C_6H_6) (C_1: type Iaa_{Bzn})	C	0.0095	0.0040	0.0013	-0.796	0.0042	71.3	90.4	0.019	68.5	32.0

[a] See Table 1 for BSSs. [b] Data are given for an interaction at BCP, which is shown by ∗ as in F–H-∗-π(C_6H_6). [c] $c\nabla^2\rho_b(\boldsymbol{r}_c) = H_b(\boldsymbol{r}_c) - V_b(\boldsymbol{r}_c)/2$, where $c = \hbar^2/8m$. [d] $k = V_b(\boldsymbol{r}_c)/G_b(\boldsymbol{r}_c)$. [e] mdyn Å^{-1}.

While θ and θ_p in X–H-∗-π(C_6H_6) are mainly controlled by the acidity of X–H, those in X–H-∗-n(OH_2) are mainly by σ*(X–H). The electron donor ability of π(C_6H_6) must be (much) weaker than that of n(OH_2), which must be responsible for the smaller θ and θ_p values in X–H-∗-π(C_6H_6), relative to those in X–H-∗-n(OH_2), together with the differences in the trends of θ and θ_p between X–H-∗-π(C_6H_6) and X–H-∗-n(OH_2).

One imaginary frequency was predicted for the optimized structure of OH_2-∗-π(C_6H_6) (C_2: type II_{Bzn}), as mentioned above, which should be examined further. Investigations on the structure and the behavior are in progress.

Conclusion

Weak X–H---π interactions in the benzene π-system will provide a very good starting point for those in various π-systems. The X–H---π(C_6H_6) adducts (X = F, Cl, Br, I, HO, MeO, H_2N, MeHN and Me_2N) were optimized with various basis set systems (BSSs) of BSS-A, BSS-B, BSS-D and/or BSS-F at the MP2 level. The optimized structures of X–H---π(C_6H_6) are summarized by the two types, type I_{Bzn} and type II_{Bzn}. Type I_{Bzn} contains the adducts constructed with only one X–H---π interaction for each. Structures are called type II_{Bzn}, if an adduct contains two H---π interactions, as in OH_2---π(C_6H_6) (C_2: type II_{Bzn}). Type I_{Bzn} is sub-divided into type I_{Bzn}, type Ia_{Bzn} and type Iaa_{Bzn} for X in X–H of monodentate halogen, bidentate oxygen and tridentate nitrogen atoms, respectively. While HO–H---π(C_6H_6) (C_s: type Ia_{Bzn}) has all positive frequencies, OH_2---π(C_6H_6) (C_2: type II_{Bzn}) contains one imaginary frequency. Consequently, the optimized structure of OH_2---π(C_6H_6) (C_2: type II_{Bzn}) should be assigned to a transition state, however, it could be assigned to a minimum, if the calculation method is suitably selected.

All BCPs expected are clearly detected in the molecular graphs drawn on the optimized structures. The X–H-∗-π(C_6H_6) interactions can be described by the linear BPs, except for MeHN–H-∗-π(C_6H_6) (C_1: type Iaa_{Bzn}) and Me_2N–H-∗-π(C_6H_6) (C_1: type Iaa_{Bzn}), of which BPs somewhat curve. Counter maps of $\rho(\boldsymbol{r})$ are drawn for the adducts. All BCPs are well located at the three-dimensional saddle points of $\rho(\boldsymbol{r})$ in the species. QTAIM-DFA was applied to the X–H-∗-π(C_6H_6) interactions. $H_b(\boldsymbol{r}_c)$ are plotted versus $H_b(\boldsymbol{r}_c) - V_b(\boldsymbol{r}_c)/2$ at BCPs of the interactions. QTAIM-DFA parameters for X–H-∗-π(C_6H_6) are calculated according to the definitions. The θ and θ_p values are less than 90º for all X–H-∗-π(C_6H_6) interactions, examined. It is concluded that all X–H-∗-π(C_6H_6) interactions are classified as the *pure* CS interactions and predicted to have the vdW character, where the standard values in the criteria are employed as a reference. The trend in

the θ and θ_p values for X–H-∗-π(C_6H_6) (X = F, Cl, Br and I) seems different from that for X–H-∗-n(OH_2). Factors to control the trend are also examined.

Acknowledgements

This work was partially supported by a Grant-in-Aid for Scientific Research (Nos. 23350019 and 26410050) from the Ministry of Education, Culture, Sports, Science and Technology, Japan. The support of the Wakayama University Original Research Support Project Grant and the Wakayama University Graduate School Project Research Grant is also acknowledged.

Notes and references

[a] *Department of Material Science and Chemistry, Faculty of Systems Engineering, Wakayama University, 930 Sakaedani, Wakayama 640-8510, Japan. Fax: +81 73 457 8253; Tel: +81 73 457 8252; E-mail: nakanisi@sys.wakayama-u.ac.jp*

† Electronic supplementary information (ESI) available: Cartesian coordinates for optimized structures of X–H---π(C_6H_6) (X = F, Cl, Br, I, HO, MeO, H_2N, MeHN and Me_2N). For ESI or other electronic format see DOI: 10.1039/b000000x.

1 L. Pauling, *The Nature of the Chemical Bond*, ed. L. Pauling, Cornell University Press, Ithaca, NY, 1960, 3rd ed., ch. 12, p. 449.
2 G. A. Jeffrey, *An Introduction to Hydrogen Bonding*, Oxford University Press: New York, 1997.
3 S. Scheiner, *Hydrogen Bonding*, Oxford University Press: New York, 1997.
4 G. R. Desiraju and T. Steiner, *The Weak Hydrogen Bond: In Structural Chemistry and Biology (IUCr Monographs on Crystallography)*, Oxford University Press: Oxford, 1999.
5 *Hydrogen Bonding and Transfer in the Excited State*, ed. K.-L. Han and G.-J. Zhao, Wiley, Chichester, 2010, vol. I and II
6 G. Gilli and P. Gilli, *The Nature of the Hydrogen Bond: Outline of a Comprehensive Hydrogen Bond Theory (IUCr Monographs on Crystallography)*, Oxford University Press: Oxford, 2009.
7 G. Gilli and P. Gilli, *The Nature of the Hydrogen Bond: Outline of a Comprehensive Hydrogen Bond Theory (IUCr Monographs on Crystallography)*, Oxford University Press: Oxford, 2009, ch. 2.3, p. 28.
8 S. Hayashi, K. Matsuiwa, M. Kitamoto and W. Nakanishi, *J. Phys. Chem. A*, 2013, **117**, 1804-1816.
9 S. N. Vinogradov and R. H. Linnell, *Hydrogen Bonding*, Van Nostrand Reinhold, New York, 1971.
10 G. R. Desiraju, *Cryst. Growth Des.,* 2011, **11**, 896-898.
11 C. B. Aakeroy and K. R. Seddon, *Chem. Soc. Rev.,* 1993, **22**, 397-407.
12 M. Meot-Ner (Mautner), *Chem. Rev.,* 2005, **105**, 213-284.
13 G. R. Desiraju, *Mol. Cryst. Liq. Cryst.,* 1992, **211**, 63-74.
14 P. Gilli and G. Gilli, *J. Mol. Struct.,* 2010, **972**, 2-10.
15 P. A. Kollman and L. C. Allen, *Chem. Rev.,* 1972, **72**, 283-303.
16 A. G. Slater, L. M. A. Perdigão, P. H. Beton and N. R. Champness, *Acc. Chem. Res.,* 2014, **47**, 3417-3427.
17 C. Otto, G. A. Thomas, K. Rippe, T. M. Jovin and W. L. Peticolas, *Biochemistry*, 1991, **30**, 3062-3069.
18 The temperature effect on the low frequency Raman spectra of hormones was investigated, which should be closely related to the specific conformation, together with the intra- and inter-molecular interactions employing QTAIM. See, V. A. Minaeva, B. F. Minaev, G. V. Baryshnikov, N. V. Surovtsev, O. P. Cherkasova, L. I. Tkachenko, N. N. Karaush and E. V. Stromylo, *Optics and Spectroscopy*, 2015, **118**, 214–223.
19 (*a*) W. Nakanishi, S. Hayashi and K. Narahara, *J. Phys. Chem. A*, 2009, **113**, 10050-10057; (*b*) W. Nakanishi, S. Hayashi and K. Narahara, *J. Phys. Chem. A*, 2008, **112**, 13593-13599.
20 W. Nakanishi and S. Hayashi, *Curr. Org. Chem.*, 2010, **14**, 181-197.
21 W. Nakanishi and S. Hayashi, *J. Phys. Chem. A*, 2010, **114**, 7423-7430.
22 A. C. Legon, P. D. Aldrich and W. H. Flygare, *J. Chem. Phys.*, 1981, **75**, 625-630.
23 P. D. Aldrich, A. C. Legon and W. H. Flygare, *J. Chem. Phys.*, 1981, **75**, 2126-2134.
24 W. G. Read, E. J. Campbell and G. Henderson, *J. Chem. Phys.*, 1983, **78**, 3501-3508.
25 J. A. Shea and S. G. Kukolich, *J. Chem. Phys.*, 1983, **78**, 3545-3551.
26 S. A. Cooke, G. K. Corlett, D. G. Lister and A. C. Legon, *J. Chem. Soc., Faraday Trans.*, 1998, **94**, 837-841.; S. A. Cooke, G. K. Corlett and A. C. Legon, *J. Chem. Soc., Faraday Trans.*, 1998, **94**, 1565-1570.
27 M. E. Sanz, S. Antolînez, J. L. Alonso, J. C. Lôpez, R. L. Kuczkowski, S. A. Peebles, R. A. Peebles, F. C. Boman, E. Kraka, D. Cremer, *J. Chem. Phys.*, 2003, **118**, 9278-9290.
28 W. G. Read, E. J. Campbell, G. Henderson and W. H. Flygare, *J. Am. Chem. Soc.*, 1981, **103**, 7670-7672; W. G. Read, E. J. Campbell and G. Henderson, *J. Chem. Phys.*, 1983, **78**, 3501-3508. See also M. E. Sanz, S. Antolinez, J. L. Alonso and J. C. Lopez, *J. Chem. Phys.*, 2003, **118**, 9278-9290.
29 S. Furutaka and S. Ikawa, *J. Chem. Phys.*, 2002, **117**, 751-755.
30 K. P. Gierszal, J. G. Davis, M. D. Hands, D. S. Wilcox, L. V. Slipchenko and D. Ben-Amotz, *J. Phys. Chem. Lett.*, 2011, **2**, 2930-2933.
31 D. A. Rodham, S. Suzuki, R. D. Suenram, F. J. Lovas, S. Dasgupta, W. A. Goddard III and G. A. Blake, *Nature*, 1993, **362**, 735-737.
32 M. Albertí, A. Aguilar, F. Huarte-Larrañaga, J. M. Lucas and F. Pirani, *J. Phys. Chem. A*, 2014, **118**, 1651-1662.
33 S. Vaupel, B. Brutschy, P. Tarakeshwar and K. S. Kim, *J. Am. Chem. Soc.*, 2006, **128**, 5416-5426.
34 X. Wang and P. P. Power, *Angew. Chem. Int. Ed.*, 2011, **50**, 10965-10968.
35 (*a*) *Atoms in Molecules. A Quantum Theory*, ed. R. F. W. Bader, Oxford University Press, Oxford, UK, 1990; (*b*) C. F. Matta and R. J. Boyd, *An Introduction to the Quantum Theory of Atoms in Molecules* In *The Quantum Theory of Atoms in Molecules: From Solid State to DNA and Drug Design*, ed. C. F. Matta and R. J. Boyd, Wiley-VCH, Weinheim, Germany, 2007, ch. 1.
36 (*a*) R. F. W. Bader, T. S. Slee. D. Cremer and E. Kraka, *J. Am. Chem. Soc.*, 1983, **105**, 5061-5068; (*b*) R. F. W. Bader, *Chem. Res.*, 1991, **91**, 893-926; (*c*) R. F. W. Bader, *J. Phys. Chem. A*, 1998, **102**, 7314-7323; (*d*) F. Biegler-König, R. F. W. Bader and T. H. Tang, *J. Comput. Chem.*, 1982, **3**, 317-328; (*e*) R. F. W. Bader, *Acc. Chem. Res.*, 1985, **18**, 9-15; (*f*) T. H. Tang, R. F. W. Bader and P. MacDougall, *Inorg. Chem.*, 1985, **24**, 2047-2053; (*g*) F. Biegler-König, J. Schönbohm and D. Bayles, *J. Comput. Chem.*, 2001, **22**, 545-559; (*h*) F. Biegler-König and J. Schönbohm, *J. Comput. Chem.*, 2002, **23**, 1489-1494.
37 J. Molina and J. A. Dobado, *Theor. Chem. Acc.*, 2001, **105**, 328-337.
38 J. A. Dobado, H. Martinez-Garcia, J. Molina and M. R. Sundberg, *J. Am. Chem. Soc.*, 2000, **122**, 1144-1149.
39 Some specific interactions are tried to analyze employing QTAIM. See, I. S. Bushmarinov, M. Y. Antipin, V. R. Akhmetova, G. R. Nadyrgulova and K. A. Lyssenko, *J. Phys. Chem. A*, 2008, **112**, 5017-5023, for an example.
40 R. J. Boyd and S. C. Choi, *Chem. Phys. Lett.*, 1986, **129**, 62-65.
41 M. T. Carroll and R. F. W. Bader, *Mol. Phys.*, 1988, **65**, 695-722.
42 S. J. Grabowski, *J. Phys. Chem. A*, 2001, **105**, 10739-10746.
43 (*a*) E. Espinosa, I. Alkorta, J. Elguero and E. Molins, *J. Chem. Phys.*, 2002, **117**, 5529-5542; (*b*) I. Rozas, I. Alkorta and J. Elguero, *J. Am. Chem. Soc.*, 2000, **122**, 11154-11161; (*c*) E. Espinosa, E. Molins and C. Lecomte, *Chem. Phys. Lett.*, 1998, **285**, 170-173.
44 M. Domagala, S. Grabowski, K. Urbaniak and G. Mloston, *J. Phys. Chem. A*, 2003, **107**, 2730-2736.
45 S. K. Ignatov, N. H. Rees, B. R. Tyrrell, S. R. Dubberley, A. G. Razuvaev, P. Mountford and G. I. Nikonov, *Chem. Eur. J.*, 2004, **10**, 4991-4999.
46 (*a*) M. Yamashita, Y. Yamamoto, K.-y. Akiba, D. Hashizume, F. Iwasaki, N. Takagi and S. Nagase, *J. Am. Chem. Soc.*, 2005, **127**, 4354-4371; (*b*) Y. Yamamoto and K.-y. Akiba, *J. Syn. Org. Chem. Jpn.*, 2004, **62**, 1128-1137.

47 S. K. Tripathi, U. Patel, D. Roy, R. B. Sunoj, H. B. Singh, G. Wolmershäuser and R. J. Butcher, *J. Org. Chem.*, 2005, **70**, 9237-9247.

48 M. Domagala and S. Grabowski, *J. Phys. Chem. A*, 2005, **109**, 5683-5688.

49 (*a*) P. Lipkowski, S. J. Grabowski and J. Leszczynski, *J. Phys. Chem. A*, 2006, **110**, 10296-10302; (*b*) M. Ziôkowski, S. J. Grabowski and J. Leszczynski, *J. Phys. Chem. A*, 2006, **110**, 6514-6521; (*c*) S. Grabowski, W. A. Sokalski and J. Leszczynski, *J. Phys. Chem. A*, 2005, **109**, 4331-4341.

50 J. Poater, M. Solâ and F. M. Bickelhaupt, *Chem. Eur. J.*, 2006, **12**, 2889-2895.

51 R. Parthasarathi, V. Subramanian and N. Sathyamurthy, *J. Phys. Chem. A*, 2006, **110**, 3349-3351.

52 D. Chopra, T. S. Cameron, J. D. Ferrara and T. N. Guru Row, *J. Phys. Chem. A*, 2006, **110**, 10465-10477.

53 W. Nakanishi, T. Nakamoto, S. Hayashi, T. Sasamori and N. Tokitoh, *Chem. Eur. J.*, 2007, **13**, 255-268.

54 R. F. W. Bader, *J. Phys. Chem. A*, 2007, **111**, 7966-7972.

55 I. S. Bushmarinov, M. Y. Antipin, V. R. Akhmetova, G. R. Nadyrgulova and K. A. Lyssenko, *J. Phys. Chem. A*, 2008, **112**, 5017-5023.

56 H. Szatylowicz, T. M. Krygowski, J. J. Panek and A. Jezierska, *J. Phys. Chem. A*, 2008, **112**, 9895-9905.

57 I. Mata, E. Molins and I. Alkorta, *J. Chem. Phys.*, 2009, **130**, 044104.

58 E. Matito and M. Solâ, *Coord. Chem. Rev.*, 2009, **253**, 647-665.

59 QTAIM-DFA is successfully applied to analyze weak to strong interactions in gas phase. It should also be applied to the interactions in crystals and to those in larger systems, containing bioactive materials, although the methodological improvement is inevitable to generate the perturbed structures suitable for the systems. Such improvement is in progress, which will be reported elsewhere.

60 S. Scheiner, *Acc. Chem. Res.*, 2013, **46**, 280-288.

61 R. T. Myers, *Inorg. Chem.*, 1977, **16**, 2671-2674.

62 A. Mukherjee, S. Tothadi and G. R. Desiraju, *Acc. Chem. Res.*, 2014, **47**, 2514-2524.

63 C. Bissantz, B. Kuhn and M. Stahl, *J. Med. Chem.*, 2010, **53**, 5061-5084.

64 Y. Umezawa, S. Tsuboyama, K. Honda, J. Uzawa and M. Nishio, *Bull. Chem. Soc. Jpn.*, 1998, **71**, 1207-1213.

65 O. Takahashi, Y. Kohno, S. Iwasaki, K. Saito, M. Iwaoka, S. Tomoda, Y. Umezawa, S. Tsuboyama and M. Nishio, *Bull. Chem. Soc. Jpn.*, 2001, **74**, 2421-2430.

66 M. Albertí, A. Aguilar, J. M. Lucas and F. Pirani, *J. Phys. Chem. A*, 2012, **116**, 5480-5490.

67 A. Jain, V. Ramanathan and R. Sankararamakrishnan, *Protein Science*, 2009, **18**, 595-605.

68 S. Tsuzuki, K. Honda, T. Uchimaru, M. Mikami and K. Tanabe, *J. Am. Chem. Soc.*, 2000, **122**, 11450-11458.

69 J. P. M. Lommerse, A. J. Stone, R. Taylor and F. H. Allen, *J. Am. Chem. Soc.*, 1996, **118**, 3108-3116.

70 J. W. G. Bloom, R. K. Raju and S. E. Wheeler, *J. Chem. Theory Comput.*, 2012, **8**, 3167-3174.

71 N. J. Singh, S. K. Min, D. Y. Kim and K. S. Kim, *J. Chem. Theor. Comput.*, 2009, **5**, 515-529.

72 Dots are usually employed to show BCPs in molecular graphs. Therefore, A-•-B would be more suitable to describe BP with BCP. Nevertheless, A-∗-B is employed to emphasize the existence of BCP on BP, in question, in our case.

73 W. Nakanishi, S. Hayashi, K. Matsuiwa and M. Kitamoto, *Bull. Chem. Soc. Jpn.*, 2012, **85**, 1293-1305.

74 θ_p and κ_p for the major bonds/interactions seem to be affected by the behavior of the bonds/interactions around those in question (minor bonds/interactions): The influence from the behavior of the minor bonds/interactions would not be so severe for usual cases. See ref 21.

75 *Gaussian 09 (Revision D.01)*, M. J. Frisch, G. W. Trucks, H. B. Schlegel, G. E. Scuseria, M. A. Robb, J. R. Cheeseman, G. Scalmani, V. Barone, B. Mennucci, G. A. Petersson, H. Nakatsuji, M. Caricato, X. Li, H. P. Hratchian, A. F. Izmaylov, J. Bloino, G. Zheng, J. L. Sonnenberg, M. Hada, M. Ehara, K. Toyota, R. Fukuda, J. Hasegawa, M. Ishida, T. Nakajima, Y. Honda, O. Kitao, H. Nakai, T. Vreven, J. A. Montgomery, Jr., J. E. Peralta, F. Ogliaro, M. Bearpark, J. J. Heyd, E. Brothers, K. N. Kudin, V. N. Staroverov, R. Kobayashi, J. Normand, K. Raghavachari, A. Rendell, J. C. Burant, S. S. Iyengar, J. Tomasi, M. Cossi, N. Rega, J. M. Millam, M. Klene, J. E. Knox, J. B. Cross, V. Bakken, C. Adamo, J. Jaramillo, R. Gomperts, R. E. Stratmann, O. Yazyev, A. J. Austin, R. Cammi, C. Pomelli, J. W. Ochterski, R. L. Martin, K. Morokuma, V. G. Zakrzewski, G. A. Voth, P. Salvador, J. J. Dannenberg, S. Dapprich, A. D. Daniels, Ö. Farkas, J. B. Foresman, J. V. Ortiz, J. Cioslowski and D. J. Fox, Gaussian, Inc.: Wallingford CT, 2009.

76 For the 6-311G(3d) basis sets, see: (a) R. C. Binning Jr. and L. A. Curtiss, *J. Comput. Chem.*, 1990, **11**, 1206-1216; (b) L. A. Curtiss, M. P. McGrath, J.-P. Blaudeau, N. E. Davis, R. C. Binning Jr. and L. Radom, *J. Chem. Phys.*, 1995, **103**, 6104-6113; (c) M. P. McGrath and L. Radom, *J. Chem. Phys.*, 1991, **94**, 511-516. For the diffuse functions (+ and ++), see: T. Clark, J. Chandrasekhar, G. W. Spitznagel and P. v. R. Schleyer, *J. Comput. Chem.*, 1983, **4**, 294-301.

77 D. Feller, *J. Comp. Chem.*, 1996, **17**, 1571-1586.

78 K. L. Schuchardt, B. T. Didier, T. Elsethagen, L. Sun, V. Gurumoorthi, J. Chase, J. Li and T. L. Windus, *J. Chem. Inf. Model.*, 2007, **47**, 1045-1052.

79 T. Noro, M. Sekiya and T. Koga, *Theoret. Chem. Acc.*, 2012, **131**, 1124.

80 (*a*) For inner and valence shells: T. Koga, S. Yamamoto, T. Shimazaki and H. Tatewaki, *Theor. Chem. Acc.*, 2002, **108**, 41-45; (*b*) For valence correlated set: M. Sekiya, T. Noro, Y. Osanai and T. Koga, *Theor. Chem. Acc.*, 2001, **106**, 297-300.

81 C. Møller and M. S. Plesset, *Phys. Rev.*, 1934, **46**, 618-622; J. Gauss, *J. Chem. Phys.*, 1993, **99**, 3629-3643; J. Gauss, *Ber. Bunsen-Ges. Phys. Chem.*, 1995, **99**, 1001-1008.

82 The AIM2000 program (Version 2.0) is employed to analyze and visualize atoms-in-molecules: F. Biegler-König, *J. Comput. Chem.*, 2000, **21**, 1040−1048. See also ref 36g.

83 The values of w = (0), ±0.1 and ±0.2 in $r = r_o + wa_o$ were employed for the perturbed structures in POM (partial optimization method),[18,19] since the bond orders becomes 2/3 and 3/2 times larger at w = +0.2 and –0.2 relative to the original value at w = 0, respectively. However, w = (0), ±0.05 and ±0.1 for $r = r_o + wa_o$ are applied in usual cases to reduce the calculation errors in the perturbed structures generated by NIV and/or POM (see also refs 19–21).

84 It is achieved by changing the corresponding parameters in Gaussian 09 from the default values to print out the normal coordinates of five digits for the purpose.

85 W. G. Read, E. J. Campbell and G. Henderson, *J. Chem. Phys.*, 1983, **78**, 3501-3508.

86 The noncovalent distances would be better reproduced by considering BSSE (basis set errors). However, optimizations are performed without considering BSSE, since the normal coordinates of internal vibrations are necessary to generate the perturbed structures in QTAIM-DFA, which are obtained through the frequency analysis.

87 S. Hayashi, Y. Sugibayashi, and W. Nakanishi, unpublished work.

88 The Chemical Handbook (Kagaku-Binran), ed. Chemical Society of Japan eds. 4th ed., Maruzen, Tokyo, in Japanese, 1993, II-315.

89 The MO energies of σ*(X–H) must be most suitable for the discussion, however, the character of σ*(X–H) seems to spread over a few vacant orbitals such as LUMO, LUMO+1 and/or LUMO+2. Therefore, ε(LUMO) of H–X is employed for the discussion.